Available online at www.sciencedirect.com

SCIENCE d DIRECT®

Journal of Catalysis ●●● (●●●●) ●●●–●●●

JOURNAL OF CATALYSIS

www.elsevier.com/locate/jcat

Reactivity of Fe-binuclear complexes in over-exchanged Fe/ZSM5, studied by in situ XAFS spectroscopy
Part 1: Heat treatment in He and O_2

A.A. Battiston, J.H. Bitter, W.M. Heijboer, F.M.F. de Groot, D.C. Koningsberger *

Department of Inorganic Chemistry and Catalysis, Debye Institute, Utrecht University, Sorbonnelaan 16, 3584 CA Utrecht, The Netherlands

Abstract

The structure of the iron species in mildly calcined over-exchanged Fe/ZSM5, prepared by CVD of $FeCl_3$, was studied during heat treatments in He or O_2/He (50:50) by coupling in situ Fe K edge HR-XANES and EXAFS. The majority of iron appears to be present as Fe-binuclear complexes. EXAFS shows that the closest Fe–O shell in the complexes can be described with a $[HO–Fe–O–Fe–OH]^{2+}$ core. Heating to a moderate temperature (up to $\sim 150\,^\circ C$) results in the desorption of water from the Fe-coordination sphere, in He as well as in a O_2/He (50:50) mixture. The composition of the gas phase strongly influences the changes occurring to the binuclear complexes in the 150–350 $^\circ C$ temperature range. Above 250 $^\circ C$ in He a significant fraction of iron undergoes autoreduction. This is accompanied by the removal of approximately one oxygen atom from the closest Fe–O shell, ascribable to the Fe–O–Fe bridging oxygen atom. The presence of oxygen in the gas phase ($PO_2 = 0.5$ bar), on the contrary, suppresses the auto-reduction capability of the binuclear complexes by inhibiting the removal of the Fe–O–Fe bridging oxygen.
© 2003 Elsevier Science (USA). All rights reserved.

Keywords: Fe/ZSM5; Binuclear; Iron; Red–ox properties; Auto-reduction; Reactivity; Helium; Oxygen

1. Introduction

Iron-exchanged ZSM5 has recently attracted considerable attention due to its ability to catalyze diverse selective oxidation reactions. Its activity has been demonstrated for the selective oxidation of benzene to phenol using N_2O [1–5], the catalytic decomposition of N_2O [6–9], and for the selective catalytic reduction of nitrogen oxides using hydrocarbons (HC-SCR) [10–12].

While the catalytic properties of iron-exchanged ZSM5 are well established, a debate is open in the literature on the nature and the reactivity of the Fe-active phase. The discussion is complicated by the fact that diverse synthesis techniques are used, resulting in different Fe/ZSM5 materials. These differences concern (i) the way by which iron is loaded (synthesis or post-synthesis methods); (ii) the chemical composition of the starting ZSM5 support (Si/Al ratio);

(iii) the amount of iron loaded; (iv) the activation treatment applied to the obtained Fe/ZSM5 (calcination, activation in vacuo or steaming).

Fe-framework substituted ZSM5, activated by calcination in vacuo or by steaming at high temperature, has shown remarkable activity towards the selective oxidation of benzene to phenol by N_2O and towards the decomposition of N_2O [1–9]. Studies by Ribera et al. [5] and Ramírez et al. [13], performed on Fe-framework substituted ZSM5, activated by steaming (~ 0.6 Fe wt%), have shown that during the activation treatment different Fe species are formed. These species vary from isolated extra framework Fe oxo-ions and oligonuclear oxo-iron complexes located in the zeolite channels to larger highly dispersed iron–oxide nanoparticles on the external surface of the zeolite. Experiments with 1,3,5-trimethylbenzene, too large to fit inside the zeolite pores, have demonstrated that the latter are not involved in the oxidation of benzene to phenol [5]. This observation supports the idea that only highly dispersed Fe species located within the zeolite channels are responsible for the peculiar selective oxidation properties of Fe/ZSM5. Panov and coworkers have ascribed the catalytic activity of this material to the

* Corresponding author.
    E-mail address: d.c.koningsberger@chem.uu.nl (D.C. Koningsberger).

yjcat3950

presence of extra-framework binuclear iron species, located in the zeolite micropores and formed by extraction of iron from the zeolite matrix during the activation treatment. By reaction with N_2O these iron centers are believed to be capable of generating a specially reactive oxygen [1–4,14–16]. This oxygen (called α-oxygen by the authors) is believed to be responsible for the oxidation of benzene to phenol already at room temperature.

Binuclear Fe oxo-hydroxo species located at the Brønsted site positions of the framework have been proposed to be the active phase also in Fe/ZSM5 prepared by the chemical vapor deposition (CVD) of anhydrous $FeCl_3$ [7,10,11,17]. Together with aqueous ion exchange [18] and solid-state ion exchange [19–24], CVD of $FeCl_3$ belongs to the so-called post-synthesis loading techniques. With the CVD technique Fe is exchanged from the gas phase at around $330\,°C$ for the H^+ Brønsted sites of an acidic Al-ZSM5 support. Final steps in the synthesis are a washing procedure, followed by drying in air and calcination in oxygen [10,25]. The as-obtained material presents major differences when compared to the activated Fe-framework substituted ZSM5, mentioned earlier. First, a significantly higher iron loading can be achieved ($\sim$ 5 Fe wt%, depending on the Si/Al ratio). Secondly, no significant damage occurs to the zeolite framework during the activation (calcination) [25]. This indicates that the formation of active Fe species does not require extraction of aluminum from the zeolite framework.

The identification of the active phase with binuclear Fe oxo-hydroxo complexes in Fe/ZSM5 by $FeCl_3$ CVD is based on results obtained by H_2 and CO TPR, FTIR, EPR, and isotopic exchange with $^{18}O_2$ [7,10,11,17,26]. The binuclear Fe complexes, with the proposed core structure $[HO–Fe–O–Fe–OH]^{2+}$, are believed to be responsible for the decomposition of N_2O [7] and for the selective reduction of NO by hydrocarbons in the presence of excess oxygen [10,11,26].

EXAFS studies performed by Marturano et al. [27,28] and by our group [25,29] have confirmed that, indeed, Fe-binuclear complexes are largely present in Fe/ZSM5 obtained by CVD. The structure of these binuclear complexes, after washing, resembles that of the closest Fe-binuclear building unit in α-goethite [25,28]. In this unit two octahedrally coordinated iron atoms are symmetrically connected via two hydroxyl groups [30,31].

A major problem in determining a structure activity relation for the active phase in Fe/ZSM5 is that for activated Fe-framework substituted ZSM5, as well as for Fe/ZSM5 prepared by $FeCl_3$ CVD, Fe species (spectators) different from binuclear complexes are present [7,17,25,26]. In particular, Fe-binuclear complexes can undergo agglomeration during calcination [25], finally resulting in the formation of catalytically inactive [3,10,24] goethite and hematite crystals on the external surface of the zeolite. However, as demonstrated in a previous study by our group [25], agglomeration of iron in Fe/ZSM5 obtained by CVD can be controlled by adequately tuning the conditions applied during calcination. Agglomer-

ation of Fe species can be significantly suppressed by applying a mild calcination procedure, obtained by coupling a moderate temperature ramp with a high gas flow rate. The resulting mildly calcined Fe/ZSM5 is, therefore, the best suited material for establishing a structure-activity relation for Fe/ZSM5 synthesized by CVD.

The objective of this work is to study the reactivity of the Fe species present in Fe/ZSM5 obtained by CVD of $FeCl_3$. The reactivity of oxygen is of particular interest since it represents the key step for the decomposition of N_2O [7], as well as for the HC-SCR of NO [10,11,17,26]. The oxidation state of iron and its local environment in a mildly calcined Fe/ZSM5 sample have been monitored during heating treatments in He and O_2, by combining the results of in situ EXAFS and high-resolution (HR)-XANES. The HR-XANES of the Fe K edge, especially the pre-edge feature (related to $1s \rightarrow 3d$ metal electronic transitions [32–34]), provides detailed information on both the oxidation state of iron and the coordination geometry [35]. This information can be used as input for the analysis of the EXAFS data. Furthermore, both HR-XANES and EXAFS benefit from the advantage of being applicable in situ, i.e., at reaction temperature and in the presence of reactants. Their combination is, therefore, a powerful tool for tracking structural changes occurring on iron during gas treatments and catalytic reactions. From the results obtained in this study a model will be proposed for the reactivity of the Fe species present in Fe/ZSM5 during heating treatments in helium and oxygen. In a subsequent paper a structure activity relation will be presented for the selective reduction of NO by hydrocarbons in the presence of excess oxygen [10,11,26].

2. Experimental

2.1. Preparation of the sample

Over-exchanged Fe/ZSM5 was prepared following the $FeCl_3$ CVD method proposed by Chen et al. [10] and extensively described in our previous work [25]. Particular attention was paid to calcination. The procedure applied (mild calcination) was identical to the procedure proposed in our previous work [25]. The sample was heated under a He flow of 800 ml/min with a moderate temperature ramp $(0.5\,°C/min)$ to $200\,°C$. At this temperature, 200 ml/min of O_2 were added to the He flow while, under the same temperature ramp, heating was continued to $550\,°C$. After 3 h at $550\,°C$, the temperature was decreased to $30\,°C$. The resulting sample, stored in air, will be referred to as Fe/ZSM5.

2.2. ICP, N_2 physisorption, XRD

The elemental composition of the starting H/ZSM5 support and of Fe/ZSM5 was determined by using inductively

ARTICLE IN PRESS

S0021-9517(02)00188-4/FLA AID:3950 Vol.●●●(●●●)   P.3(1-15)
ELSGMLTM(JCAT):m5 2003/03/18 Prn:18/03/2003; 11:18   by:Viktorija p. 3

yjcat3950

A.A. Battiston et al. / Journal of Catalysis ●●● (●●●●) ●●●–●●●   3

coupled plasma emission spectroscopy. 0.10 g of the samples were mixed in a platinum cup together with 0.40 g of Li-tetraborate and 0.20 g of Li-metaborate and heated to 925 °C. This temperature was maintained for 1 h. After cooling, the resulting soluble borate was dissolved in 330 ml HCl (1.0 M), diluted to 1000 ml with doubly deionized water, and analyzed.

The micropore volume of the acidic support and of Fe/ZSM5 (after washing and after calcination) was determined by N_2 physisorption, using a Micromeritics ASAP 2010, as described in [25]. N_2 physisorption data obtained on sample Fe/ZSM5 were corrected for the additional metal loading (~ 4.4 wt%) for comparison with the H/ZSM5 support.

XRD diffractograms obtained from the acidic support and from the Fe/ZSM5 sample (after washing and after calcination) were compared to visualize possible lattice damage or formation of additional Fe-rich crystalline phases. X-ray diffraction patterns were recorded using a Nonius PDS 120 powder diffractometer. The radiation used was Co-K_{α_1} ($\lambda = 1.78897$ Å). Diffractograms were recorded for 24 h and averaged in order to optimize the signal-to-noise ratio.

2.3. Fe K-edge HR-XANES

High-resolution X-ray Absorption Near Edge Spectroscopy was applied in order to study the oxidation state and the coordination geometry of Fe in Fe/ZSM5. This information was obtained by analyzing the features (centroid position and integrated intensity) of the Fe K pre-edge, located 15–20 eV before the main Fe K-edge crest. The HR-XANES measurements at the Fe K edge were carried out at the undulator beamline ID16 at the ESRF (Grenoble, France). Details about the experimental setup are given in [36] and in our previous paper [25].

2.3.1. HR-XANES data collection

Fe/ZSM5 was pressed into self-supporting wafers and placed in an in situ fluorescence cell [37] at 45° with respect to the beam. Spectra were recorded at 1 bar during heating treatments from 30 to 350 °C (heating ramp of 3 °C/min). The heating treatments were performed under different atmospheres, i.e., flowing He (100 ml/min) or a 50:50 He/O_2 flowing mixture (total flow = 100 ml/min). The sample heated up in He, after 30 min stabilization (under flowing He) at 350 °C, was flushed with a 50:50 He/H_2 mixture (total flow = 100 ml/min, $T = 350$ °C) and measured after 15 min under the same conditions. Hematite was measured under static He at 30 °C as internal reference.

2.3.2. HR-XANES data processing

The fluorescence Fe K XANES spectra were normalized by the average absorption intensity, calculated in the 7200–7300 eV region. To isolate the pre-edge feature, the contribution to the pre-edge of the main Fe K edge was subtracted from the normalized XANES spectra. This contribution was calculated using a cubic spline function, obtained by interpolating the data several eV before and after the pre-edge [35].

The recorded HR-XANES spectra revealed the presence of fluorescence saturation effects. This was revealed by comparing the maximum intensity of the isolated pre-edges of the normalized HR-XANES spectra measured in fluorescence with those measured (on the same samples) in transmission mode at beamline X1.1 at Hasylab (vide infra). Nevertheless, numerical comparison showed that, as far as the pre-edge is concerned, it was possible to correct for the saturation effects by dividing the maximum intensity of the isolated fluorescence pre-edges by that of the corresponding pre-edges measured in transmission. This procedure was performed independently on the hematite reference and on sample Fe/ZSM5, measured at 30 °C in He. The correction factor obtained for Fe/ZSM5 measured at 30 °C in He was used to normalize also the pre-edge data of Fe/ZSM5 measured at higher temperatures and in different environments (He/O_2, He/H_2). The rightness of the correction applied was further confirmed by using the procedure outlined in [38], based on intensity dependent correction of the occurring saturation.

The characteristics of the isolated pre-edges, i.e., centroid position and integrated intensity were calculated using the Grams software. Prior to calculations, the pre-edge of α-Fe_2O_3 (not shown here, see [25]) was deconvoluted into pseudo-Voigt components (50% Gaussian, 50% Lorentzian peak shapes). The contribution from components centered above 7115.0 eV was ignored [32,35]. The estimated accuracy in the energy determination for the HR-XANES spectra presented in this study is ± 0.05 eV, while the error in the integrated intensity is ± 5%.

2.4. Fe K-edge XAFS

Fe K-edge XAFS was applied in order to study the Fe-oxidation state and the local atomic environment around iron, i.e., number, distances, and chemical nature of Fe neighbors. The XAFS data were collected at the Wiggler station X1.1 of Hasylab (Hamburg, Germany). The experimental setup is described in [25].

2.4.1. XAFS data collection

Fe/ZSM5 was pressed to obtain self-supporting wafers, calculated to have an absorbency ($\mu * x$) of 2.5, and placed in a controlled atmosphere cell. The cell is similar to that used for the HR-XANES fluorescence measurements and is described in detail elsewhere [37]. The samples were treated in situ under flowing He (50 ml/min) or under a 50:50 O_2/He mixture (total flow of 50 ml/min). They were heated under the mentioned flows to 120 or 350 °C, applying a temperature ramp of 5 °C/min. Spectra were recorded at working temperature (under flowing atmospheres) or, with the cell closed, after being cooled to 77 K. A list of the measurements performed on sample Fe/ZSM5, including informa-

ARTICLE IN PRESS

S0021-9517(02)00188-4/FLA AID:3950 Vol.●●●(●●●)
ELSGMLTM(JCAT):m5 2003/03/18 Prn:18/03/2003; 11:18

yjcat3950

P.4(1-15)
by:Viktorija p. 4

4

Table 1
List of XAFS spectra recorded from Fe/ZSM5: pretreatments and measuring conditions

Pretreatments (flowing atmosphere)	Environ. conditions during measurement	Aver. scans	Measurements code
He, 15 min, 30 °C	Static He, 77 K	3	Fe/ZSM5-He 30 °C/LN
↑ He, 30 min at 120 °C	Static He, 77 K	3	Fe/ZSM5-He 120 °C/LN
↑ He, 30 min at 350 °C	Flowing He, 350 °C	1	Fe/ZSM5-He 350 °C (1st)/350 °C
↑ He, 60 min at 350 °C	Flowing He, 350 °C	1	Fe/ZSM5-He 350 °C (2nd)/350 °C
↑ He, 90 min at 350 °C	Flowing He, 350 °C	1	Fe/ZSM5-He 350 °C (3rd)/350 °C
↑ He, 120 min at 350 °C	Static He, 77 K	3	Fe/ZSM5-He 350 °C/LN
↑ O_2/He, 60 min at 350 °C	Flowing O_2/He, 350 °C	3	Fe/ZSM5-O_2 350 °C/350 °C
↑ O_2/He, 120 min at 350 °C	Static O_2/He, 77 K	3	Fe/ZSM5-O_2 350 °C/LN

↑ = Heating treatment (5 °C/min).

tion on pretreatments, measuring conditions, number of averaged scans, and measurements codes, is given in Table 1. XANES spectra of hematite and Fe–titanate were also measured and used, respectively, as internal Fe^{III} and Fe^{II} references.

2.4.2. XAFS data processing

Extraction of the EXAFS data from the measured absorption spectra was performed with the XDAP code developed by Vaarkamp et al. [39]. Three scans were recorded for each measurement and averaged. In the case of significant differences between the three scans, spectra were analyzed separately (see Table 1, scans Fe/ZSM5-He 350 °C (1st, 2nd, 3rd)/350 °C). The pre-edge was subtracted using a modified Victoreen curve [40]. The background was subtracted employing cubic spline routines with a continuously adjustable smooth parameter [41,42]. Normalization was performed by dividing the data by the intensity of the absorption spectrum at 50 eV above the Fe K edge.

2.4.3. EXAFS Fe–O, Fe–Fe references, data analysis

The Fe–O reference used for the EXAFS data analysis was created from experimental EXAFS data, obtained from ferric acetylacetonate (measured at L.N. temperature). The Fe–Fe phase shifts and backscattering amplitudes were calculated using the software FEFF7 [43]. The theoretical Fe–Fe reference was calibrated on EXAFS data obtained from hematite at L.N. temperature, by fitting in R space. The complete procedure followed for the creation and the calibration of the EXAFS Fe–O and the Fe–Fe references is reported in [25].

The EXAFS data analysis was performed by applying multiple-shell fitting in R space [41]. The difference file technique was applied to resolve the different contributions in the EXAFS data. The EXAFS fits were checked by applying k^1, k^2, and k^3 weightings.

The number of independent fit parameters (N_{indp}) was determined by equation

$$N_{indp} = \frac{2\Delta k \Delta R}{\pi} + 2, \tag{1}$$

as outlined in the Reports on Standard and Criteria in XAFS Spectroscopy [44]. Errors in the numerical values obtained

Table 2
Elemental composition (ICP) and micropore volume (N_2 physisorption) of H/ZSM5 (starting support) and of Fe/ZSM5, after washing (Fe/ZSM5-w) and after washing followed by a mild calcination (Fe/ZSM5-w + mc)

Samples	Si/Al (atomic ratio)	Fe/Al (atomic ratio)	Micropore volume (cm^3/$g_{support}$)
H/ZSM5	17.0	0.0	0.15
Fe/ZSM5-w	17.4	1.0	0.12
Fe/ZSM5-w + mc	17.2	1.0	0.12

by the EXAFS data analysis are estimated to be ±10% in the coordination number (N), ±1% in the distance (R), ±5% in the Debye–Waller factor ($\Delta\sigma^2$), and ±10% in the inner potential correction (ΔE_0) [45].

3. Results

3.1. ICP, N_2 physisorption, XRD

Table 2 shows the elemental composition and the micropore volume of the parent H/ZSM5 support and of the Fe/ZSM5 sample after washing, and upon mild calcination. The Si/Al ratio in the starting support and in the obtained Fe/ZSM5 is, within the margin of error, the same. This result shows that no aluminum was leached out during the synthesis [25]. The Fe/Al of 1.0 is a typical result of the $FeCl_3$ CVD technique, by which a complete exchange of Fe^{III} for the Brønsted protons of the support is obtained. It should nevertheless be noted that, as shown in previous works [21,25,27], partial removal of Fe from the Brønsted sites may occur during washing and calcination.

After the loading of iron, a decrease of around 20% was detected in the micropore volume of the ZSM5 support (Fe/ZSM5-w). No further changes were visible upon mild calcination. This shows that applying a mild calcination procedure does not result in significant removal of iron to the external surface of the zeolite. This observation was confirmed by HR-TEM measurements shown in [25].

X-ray diffractograms (not shown), collected after the subsequent steps of the Fe/ZSM5 synthesis, did not show any change in the diffraction peaks. This indicates that no

ARTICLE IN PRESS

S0021-9517(02)00188-4/FLA   AID:3950   Vol.●●●(●●●)   P.5(1-15)
ELSGMLTM(JCAT):m5 2003/03/18 Prn:18/03/2003; 11:18   yjcat3950   by:Viktorija p. 5

A.A. Battiston et al. / Journal of Catalysis ●●● (●●●●) ●●●–●●●   5

detectable damage to the ZSM5 framework is observed, nor the presence of additional Fe oxidic or oxo-hydroxidic crystalline phases.

3.2. Fe K-edge HR-XANES

Fig. 1a shows the normalized background subtracted high-resolution pre-edges isolated from the HR-XANES spectra of Fe/ZSM5, measured during the heating treatment in helium. By increasing the temperature from 30 to 130 °C a clear enhancement was detected in the pre-edge intensity, while no significant shift was visible in the pre-edge posi-
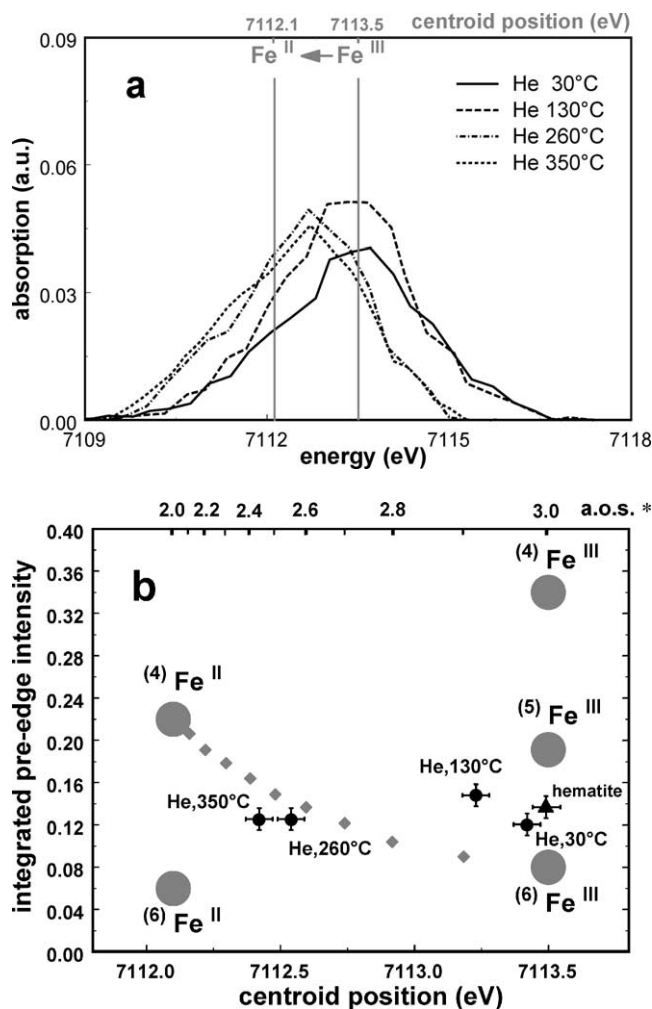

Fig. 1. (a) Normalized high-resolution background substracted pre-edge spectra of Fe/ZSM5, measured during heat treatment in He (1 bar, 100 ml/min, heating ramp 3 °C/min); (b) Summary of pre-edge characteristics (centroid position and integrated intensity) of Fe/ZSM5 (●), measured during heating treatment in He. Pre-edge characteristics of $^{(6)}Fe^{III}$, $^{(5)}Fe^{III}$, $^{(4)}Fe^{III}$, $^{(6)}Fe^{II}$, $^{(4)}Fe^{II}$ (⬤) and $^{(6)}Fe^{III}/^{(4)}Fe^{II}$ binary mixtures (◆), obtained from the literature [35], are reported for comparison, together with the experimental pre-edge features of hematite (▲). The diagram does not consider five-coordinated Fe^{II}/Fe^{III} combinations, as well as ternary or more complex mixtures. * The average oxidation number of the $^{(6)}Fe^{III}/^{(4)}Fe^{II}$ binary mixtures is reported in the upper x-axis against the corresponding energy of the centroid positions (lower x-axis).

tion. An additional increase of the temperature to 260 °C caused a clear shift of the pre-edge toward lower energy, accompanied by only a slight decrease in the maximum intensity and in the area (integrated intensity) of the pre-edge. Reaching the final temperature of 350 °C resulted in an additional minor shift toward lower energy, while no further changes were measured in the pre-edge area.

The characteristics (integrated intensity vs centroid position) of the pre-edges of Fe/ZSM5, measured during the heating treatment in helium, are plotted in Fig. 1b with small black dots. This figure also gives the pre-edge features of well-defined Fe–crystalline materials, with known Fe-oxidation state and coordination geometry. Here II and III give the Fe oxidation states, while the number between brackets in the superscript represents the number of oxygen neighboring atoms. Single-phase Fe compounds are indicated with large gray dots, while binary mixtures of $^{(6)}Fe^{III}/^{(4)}Fe^{II}$ are plotted with small gray lozenges. As a comparison, the results obtained for hematite measured in He at 30 °C are also shown, depicted with a triangle.

The pre-edge features of the Fe references have been obtained from the work of Wilke et al. [35]. In their work the authors have shown that, irrespectively of the coordination geometry, the centroid position of Fe^{II} and Fe^{III} are separated by 1.4 ± 0.1 eV and are positioned at 7112.1 and 7113.5 eV, respectively. At a given oxidation state, the lowest pre-edge integrated intensity corresponds to the most centrosymmetric coordination of iron ($^{(6)}Fe$). A decrease in symmetry, as well as in the number of coordinated neighbors ($^{(6)}Fe \rightarrow {}^{(4)}Fe$), results in an increase of the pre-edge integrated intensity. The variation in pre-edge intensity is larger for Fe^{III} compounds.

The results of Wilke et al. obtained for binary mixtures of $^{(6)}Fe^{III}/^{(4)}Fe^{II}$ are important to understand the changes in the coordination geometry of Fe in Fe/ZSM5, as a function of the heat treatment in He. The authors have systematically varied the $^{(6)}Fe^{III}/^{(4)}Fe^{II}$ molar ratio of a binary mixture. In their XANES study they determined the centroid position and the integrated intensity of the pre-edge feature of the different mixtures. The average oxidation state of the $^{(6)}Fe^{III}/^{(4)}Fe^{II}$ binary mixtures is given here in the upper x-axis as a function of the corresponding energy of the centroid positions (lower x-axis). It should be noted that the average red–ox state and integrated intensity of iron varies non linearly with the pre-edge position. This phenomenon is caused by the different contributions to the pre-edge intensity from tetrahedrally and octahedrally coordinated Fe atoms.

By comparing the data obtained for Fe/ZSM-5 with those of the references, it can be concluded that iron in Fe/ZSM5 measured in He at 30 °C is present as slightly distorted octahedrally coordinated Fe^{III}. Its oxidation state and coordination geometry appear, indeed, to be very similar to that of the hematite reference. By heating Fe/ZSM5 in He to 130 °C an increase is visible in the pre-edge integrated intensity, while only a slight shift (-0.2 eV)

yjcat3950

of the centroid position is observed. The main effect of moderate heating in He is a decrease in symmetry or/and in the number of neighbors coordinated to iron, without a significant reduction in the average Fe-oxidation state. A plausible interpretation for these results appears to be the incipient removal of water molecules from the coordination of iron.

An additional increase of the temperature to 260 °C caused a clear shift of the pre-edge (-0.7 eV), together with only a slight decrease of its integrated intensity. As can be seen in Fig. 1b, the features of the pre-edge at 260 °C in He appear to be similar to that of a 50:50 $^{(6)}Fe^{III}/^{(4)}Fe^{II}$ mixture. Although only qualitative conclusions can be deduced, the results clearly show the onset, above 130 °C, of reduction phenomena involving a considerable fraction of iron. The reduction is accompanied by an additional decrease in the average Fe-coordination number. This can be ascribed to a further desorption of water and, coherently with the chemical reduction of iron, to removal of oxygen. The features of the pre-edge appear to be only slightly affected (additional slight reduction) by an increase of the temperature from 260 to 350 °C.

Fig. 2a shows the normalized high-resolution background subtracted pre-edges of Fe/ZSM5, measured during heating in oxygen from 30 to 350 °C ($O_2/He = 50:50$). The pre-edge measured in He at 30 °C is also given for comparison. Heating Fe/ZSM5 in oxygen to 160 °C resulted in a strong increase in the pre-edge intensity. This increase is almost identical to that measured under He at 130 °C (see Fig. 1a). Increasing the temperature further to 350 °C did not cause any major change with respect to both the pre-edge position and its intensity. These results are visualized in Fig. 2b. Heating in the presence of oxygen caused a decrease in the centrosymmetry of Fe but did not result in chemical reduction of Fe. This can be ascribed to the removal of coordinated water molecules. As can be seen, the average Fe pre-edge features measured on Fe/ZSM5 in oxygen at 350 °C resembles those of five-fold coordinated Fe^{III}.

Completely different results were obtained on the Fe pre-edge measured in H_2 at 350 °C, after preheating in He at the same temperature (see Fig. 2a). The pre-edge is clearly shifted to lower energy (-1.3 eV, when compared to the reference sample) and its integrated intensity appears to be increased. The pre-edge characteristics in H_2 at 350 °C are very close to that of tetrahedrally coordinated Fe^{II}, as depicted in Fig. 2b. Thus, the reduction process affected almost all of the Fe atoms in sample Fe/ZSM5.

3.3. Fe K-edge XAFS

3.3.1. Heat treatment in He

The effects of the heating treatment in He on the oxidation state of iron are visualized in Fig. 3a. The picture shows the XANES spectra of Fe/ZSM5, measured at liquid nitrogen temperature after treatment in He at 30 °C, 120 °C, and at 350 °C (after 120 min stabilization). The XANES spectra
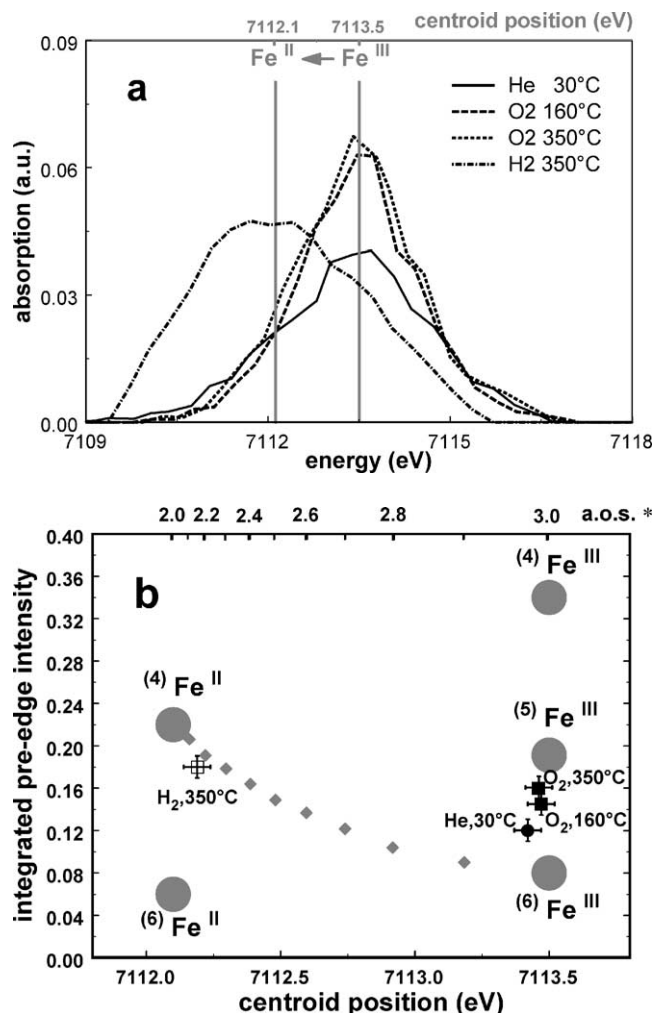

Fig. 2. (a) Normalized high-resolution background substracted pre-edge spectra of Fe/ZSM5, measured during heat treatment (heating ramp of 3 °C/min) in oxygen (1 bar, 100 ml/min, $O_2/He = 50:50$), and measured in hydrogen (1 bar, 100 ml/min, $H_2/He = 50:50$) at 350 °C, after heat treatment in He to 350 °C (1 bar, 100 ml/min, heating ramp of 3 °C/min). (b) Summary of pre-edge characteristics of Fe/ZSM5 measured at 30 °C in helium (●), during heat treatment in oxygen (■), and measured in hydrogen at 350 °C (□) after heat treatment in He to 350 °C. For details on Fe references [35] see the caption to Fig. 1b.

of hematite and Fe–titanate are also reported, respectively, as internal Fe^{III} and Fe^{II} references. As can be seen from the picture, the Fe K-edge position of Fe/ZSM5 at 30 °C corresponds to that of hematite (Fe^{III}). Consistently with what observed by HR-XANES, heating to 120 °C does not result in reduction of iron. A real reduction is observed only upon heating in He to 350 °C.

Fig. 3b shows the experimental EXAFS data (measured in He at 77 K) of Fe/ZSM5-He 30 °C/LN (solid line), Fe/ZSM5-He 120 °C/LN (dotted line), and Fe/ZSM5-He 350 °C/LN (dashed line). Sample Fe/ZSM5-He 350 °C/LN was measured after 120 min stabilization in He at 350 °C. Fig. 3b shows that both the EXAFS amplitude and the nodes in k space are affected by the treatment in He, thus heating in He resulted in significant changes affecting the

ARTICLE IN PRESS

S0021-9517(02)00188-4/FLA AID:3950 Vol.●●●(●●●)
ELSGMLTM(JCAT):m5 2003/03/18 Prn:18/03/2003; 11:18

yjcat3950

P.7(1-15)
by:Viktorija p. 7

A.A. Battiston et al. / Journal of Catalysis ●●● (●●●●) ●●●–●●●

7

Table 3
Coordination parameters obtained by R-space analysis (k^1, $\Delta k = 2.7$–13.2 Å^{-1}; $\Delta R = 0.7$–4.2 Å) of EXAFS data of Fe/ZSM5-He 30 °C/LN

Shells	N	R (Å)	$\Delta\sigma^2$ (10^{-3} Å^2)	ΔE_0 (eV)	k^1-Variance (%)	
	($\pm 10\%$)	($\pm 1\%$)	($\pm 5\%$)	($\pm 10\%$)	Im. part	Abs. part
Fe/ZSM5-He 30 °C/LN (model 2:2:2)					0.46	0.41
Fe–O$_1$	1.9	1.86	−3.9	0.5		
Fe–O$_2$	2.0	1.97	−5.0	13.4		
Fe–O$_3$	2.1	2.09	−1.0	−6.8		
Fe–Fe$_1$	1.2	3.05	5.9	−3.2		
Fe–Fe$_2$	0.4	3.40	14.2	−5.5		
Fe–O$_z$	4.5	4.01	15.0	−5.0		
Fe/ZSM5-He 30 °C/LN (model 3:3)					0.38	0.36
Fe–O$_1$	3.0	1.90	9.6	12.0		
Fe–O$_2$	3.1	2.04	4.3	−7.3		
Fe–Fe$_1$	1.2	3.06	5.4	−3.6		
Fe–Fe$_2$	0.4	3.40	10.7	−8.0		
Fe–O$_z$	4.7	4.11	11.7	−6.6		

Model (2:2:2): $N_{\text{indp}} = 25.4$; $N_{\text{free (fit)}} = 22$.
Model (3:3): $N_{\text{indp}} = 25.4$; $N_{\text{free (fit)}} = 18$.

local environment of iron. These changes are also revealed in the corresponding Fourier transforms of the experimental EXAFS data (Fig. 3c). Three main peaks are visible, centered, respectively, at around 1.5 Å (Fe–O, in the picture), 2.6 Å (Fe–Fe$_1$), and 3.1 Å (Fe–Fe$_2$). It can be seen that the largest changes occur after heating in He at temperatures higher than 120 °C. Large changes can be observed in the Fe–O shells region in the range $1.0 < R < 2.0$ Å. Also the Fe–Fe$_1$ shell is influenced.

The EXAFS coordination parameters obtained by the R-space fitting procedure for sample Fe/ZSM5-He 30 °C/LN are collected in Table 3. For the R-space fit the Fourier transform range was taken from 2.7 to 13.2 Å^{-1} with a range in R space from 0.7 to 4.2 Å. The number of independent parameters was calculated to be $N_{\text{indp}} = 25.4$. Consistently with the results obtained by HR-XANES on Fe/ZSM5 measured at 30 °C, the fit of the Fe–O contribution revealed the presence of six oxygen neighbors. A good quality fit could be obtained with two different oxygen distributions, i.e., by using two oxygen shells (model 3:3) or three oxygen shells (model 2:2:2). The total number of fit parameters was 18 and 22, respectively. No significant difference was obtained in the statistical variance of the two fits. It should be noted that for both models the fits were optimized by including distant oxygen neighbors, attributed to the zeolite framework (Fe–O$_z$). No further implications for a structural model were derived from this Fe–O$_z$ contribution, added to the fit in order to analyze more reliably shell Fe–Fe$_2$ (vide infra).

The second peak of the Fourier transform (Fe–Fe$_1$) was fitted with a Fe–Fe shell at 3.05 Å with a coordination number of 1.2. This shell is ascribed to the presence of binuclear Fe complexes [25]. The fact that the coordination number of this shell is higher than 1.0 and that an additional Fe–Fe$_2$ shell could be fitted at higher distances ($R = 3.40$ Å,
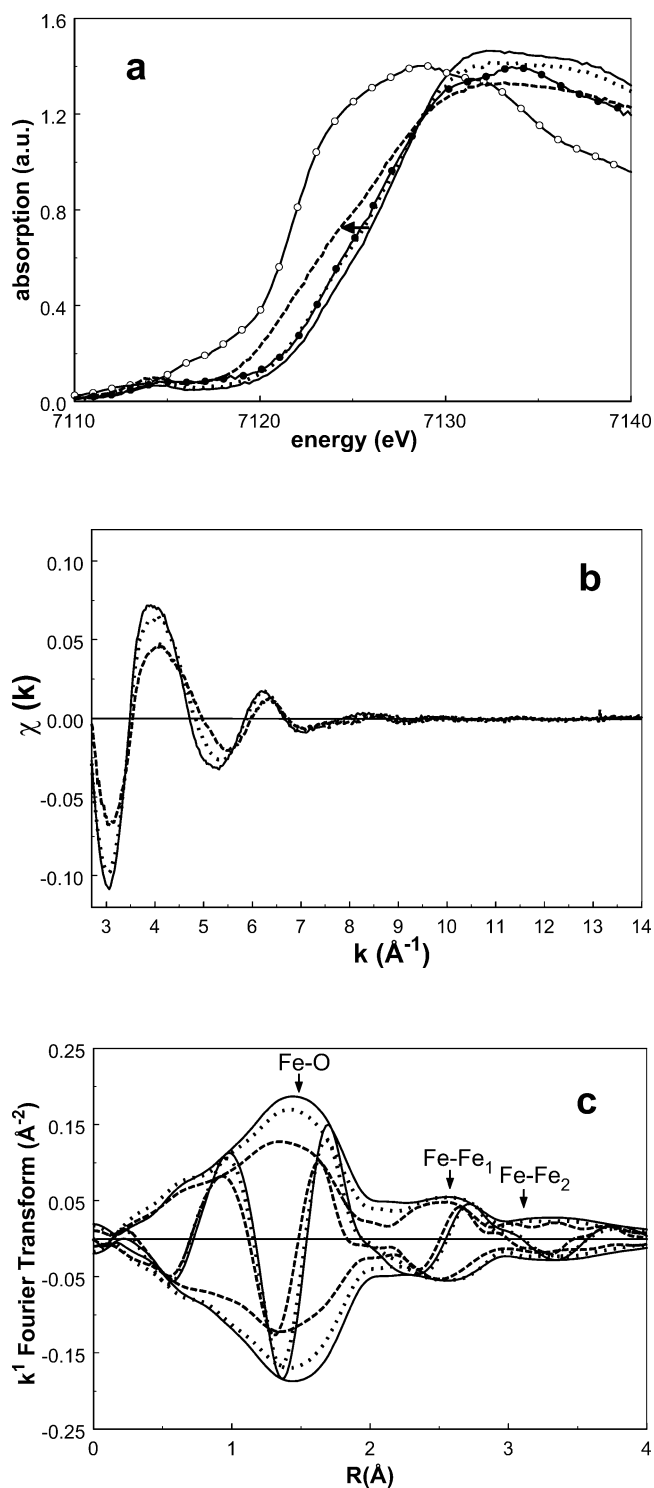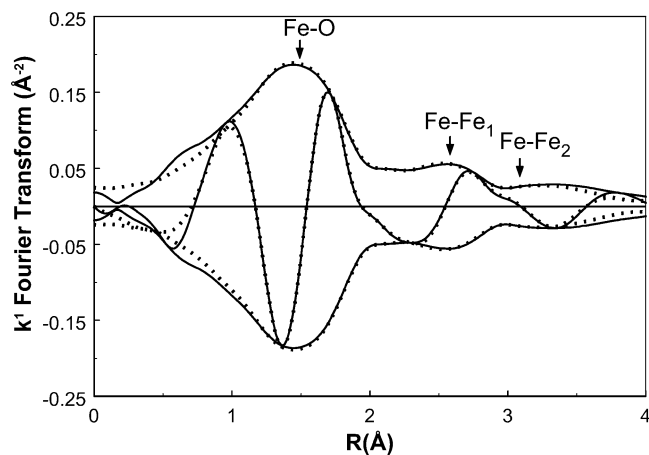
Fig. 3. (a) Normalized XANES spectra of Fe/ZSM5-He 30 °C/LN (solid line), Fe/ZSM5-He 120 °C/LN (dotted line), Fe/ZSM5-He 350 °C/LN (dashed line). Sample Fe/ZSM5-He 350 °C/LN was measured after 120 min stabilization in He at 350 °C. Normalized XANES spectra of hematite (●, solid line) and Fe–titanate (○, solid line) are also reported, respectively, as internal Fe^{III} and Fe^{II} references. (b) Experimental $\chi(k)$ data measured as a function of the heat treatment in He: Fe/ZSM5-He 30 °C/LN (solid line), Fe/ZSM5-He 120 °C/LN (dotted line), Fe/ZSM5-He 350 °C/LN (dashed line). (c) Fourier transform (k^1, $\Delta k = 2.7$–13.2 Å^{-1}) of EXAFS data of Fe/ZSM5-He 30 °C/LN (solid line), Fe/ZSM5-He 120 °C/LN (dotted line), and Fe/ZSM5-He 350 °C/LN (dashed line).

ARTICLE IN PRESS

S0021-9517(02)00188-4/FLA   AID:3950   Vol.●●●(●●●)
ELSGMLTM(JCAT):m5 2003/03/18 Prn:18/03/2003; 11:18

yjcat3950

P.8 (1-15)
by:Viktorija p. 8

Fig. 4. Fourier transform (k^1, $\Delta k = 2.7–13.2$ Å^{-1}) of EXAFS data of Fe/ZSM5-He 30 °C/LN (solid line) and R-space fit (dotted line; $0.7 < R$ (Å) < 4.2; fit-model 2:2:2).

$N = 0.4$), as already discussed in [25], is the result of further agglomeration of a fraction of iron. From the EXAFS coordination numbers of the Fe–Fe shells, binuclear clusters in sample Fe/ZSM5 are estimated to account for at least 70% of the total iron [25]. The quality of R-space fit using the 2:2:2 model is demonstrated in Fig. 4 for the Fe/ZSM5 sample treated in He at 30 °C RT and measured at L.N. temperature.

The results obtained during the heat treatments can be best described and understood in terms of the 2:2:2 model. The reactivity of the Fe/ZSM5 sample, using the 2:2:2 model, is visualized in changes in the number of oxygen neighbors in the Fe–O$_1$ and Fe–O$_3$ coordination.

The results of the R-space fits of measurements Fe/ZSM5-He 30 °C/LN, Fe/ZSM5-He 120 °C/LN, and Fe/ZSM5-He 350 °C/LN, using the 2:2:2 model, are summarized in Table 4. It can be seen that the coordination number of the Fe–O$_3$ coordination significantly decreases with increasing temperature from 2.1 (30 °C) to 1.4 (120°), and to 0.9 (350 °C). As a result, the imaginary part of the total Fe–O contribution appears to be shifted toward lower R (Fig. 3c). Since the EXAFS analysis showed already a decrease in the coordination number of the Fe–O$_3$ shell at 120 °C (Fe-oxidation state is III), the oxygen located in this shell cannot be responsible for red–ox behavior of iron. The Fe–O$_3$ shell is therefore attributed to weakly bound oxygen, most probably of H$_2$O. Besides a further decrease in the oxygen coordination number, an increase in the disorder ($\Delta\sigma^2$) and a change in the inner potential value (ΔE_0) of the Fe–O$_3$ shell is observed when heating from 120 to 350 °C. At the same time a small decrease is visible in the coordination number of the Fe–O$_1$ shell. The decrease of the oxygen coordination number of the Fe–O$_3$ shell as a function of the He treatment is visualized in Fig. 5. No changes are observed for the Fe–O$_2$ shell during the heat treatment in He.

Also a change in the distance of the Fe–Fe$_1$ is observed when heating from 120 to 350 °C, indicating a shortening in

Table 4
Coordination parameters (model 2:2:2) obtained by R-space analysis (k^1, $\Delta k = 2.7–13.2$ Å^{-1}; $\Delta R = 0.7–4.2$ Å) of EXAFS data of Fe/ZSM5-He 30 °C/LN, Fe/ZSM5-He 120 °C/LN, and Fe/ZSM5-He 350 °C/LN

| Shells	N	R (Å)	$\Delta\sigma^2$ (10^{-3} Å^2)	ΔE_0 (eV)	k^1-Variance (%)	
	($\pm10\%$)	($\pm1\%$)	($\pm5\%$)	($\pm10\%$)	Im. part	Abs. part
Fe/ZSM5-He 30 °C/LN					0.46	0.41
Fe–O$_1$	1.9	1.86	−3.9	0.5		
Fe–O$_2$	2.0	1.97	−5.0	13.4		
Fe–O$_3$	2.1	2.09	−1.0	−6.8		
Fe–Fe$_1$	1.2	3.05	5.9	−3.2		
Fe–Fe$_2$	0.4	3.40	14.2	−5.5		
Fe–O$_z$	4.5	4.01	15.0	−5.0		
Fe/ZSM5-He 120 °C/LN					0.49	0.37
Fe–O$_1$	2.0	1.85	−3.9	0.5		
Fe–O$_2$	2.0	1.97	−5.0	13.4		
Fe–O$_3$	1.4	2.09	−2.2	−6.8		
Fe–Fe$_1$	1.2	3.05	2.9	−3.2		
Fe–Fe$_2$	0.4	3.40	14.2	−5.5		
Fe–O$_z$	4.5	4.01	15.0	−5.0		
Fe/ZSM5-He 350 °C/LN					0.58	0.55
Fe–O$_1$	1.8	1.85	−3.5	−1.8		
Fe–O$_2$	2.0	1.97	−4.3	12.6		
Fe–O$_3$	0.9	2.08	2.2	−11.1		
Fe–Fe$_1$	1.2	2.97	1.3	1.8		
Fe–Fe$_2$	0.4	3.40	15.0	−5.5		
Fe–O$_z$	3.2	3.99	15.0	−4.9		

$N_{indp} = 25.4$; $N_{free \, (fit)} = 22$.
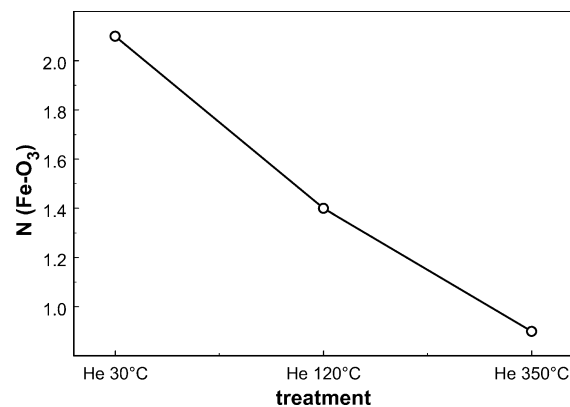
Fig. 5. Average number of oxygen atoms in the Fe–O$_3$ coordination shell (model 2:2:2) as a function of heat treatment in He.

the Fe–Fe distance of the binuclear Fe complexes (2.97 Å in He at 350 °C). During the fitting process, the coordination number and distance of the Fe–Fe$_2$ shell were fixed to the values obtained for measurement Fe/ZSM5-He 30 °C/LN (model 3:3). Fe–Fe$_2$ is a minor contribution and no important information was derived from this shell for the autoreduction properties of the Fe/ZSM5 sample.

3.3.2. Stabilization in He at 350 °C

The results presented above for the He treatment at 350 °C were obtained after 120 min stabilization on stream and after cooling the Fe/ZSM5 sample to liquid nitrogen
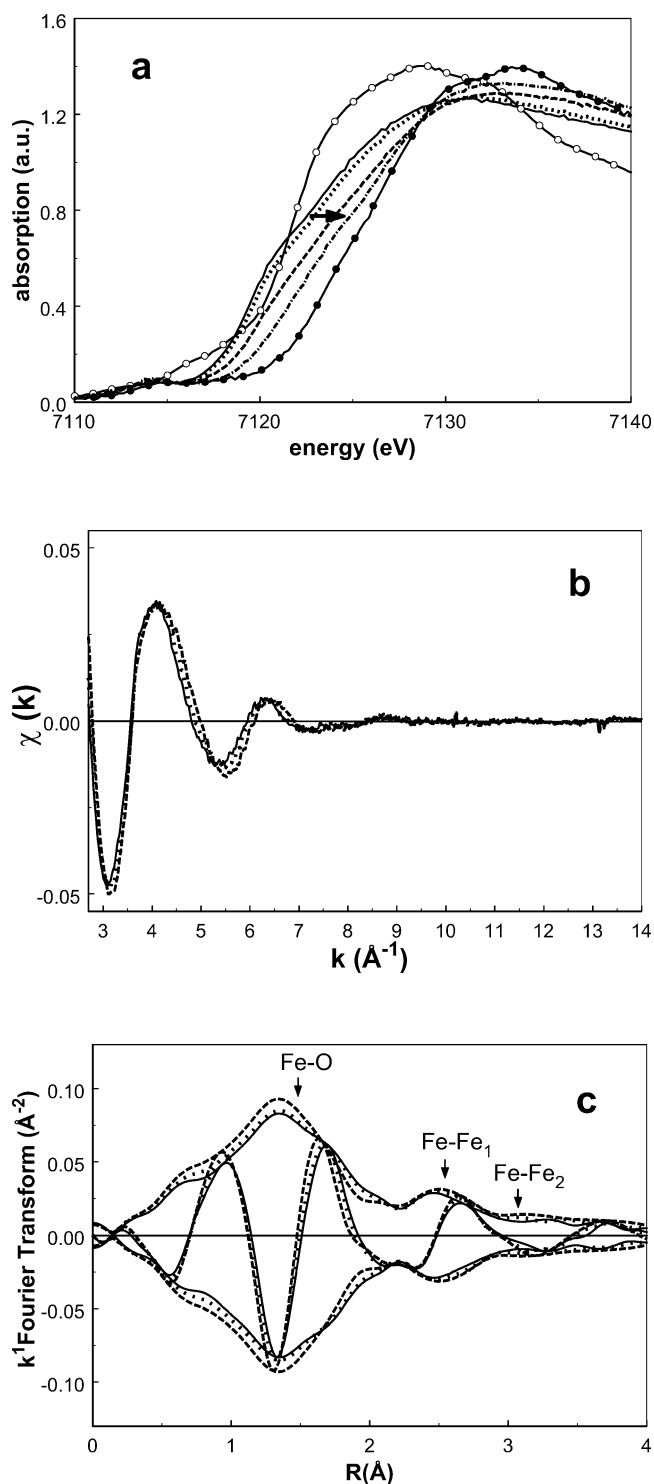
ARTICLE IN PRESS

S0021-9517(02)00188-4/FLA   AID:3950   Vol.●●●(●●●)   yjcat3950   P.9 (1-15)
ELSGMLTM(JCAT):m5 2003/03/18 Prn:18/03/2003; 11:18   by:Viktorija p. 9

A.A. Battiston et al. / Journal of Catalysis ●●● (●●●●) ●●●–●●●   9

Fig. 6. (a) Normalized XANES spectra of Fe/ZSM5-He 350 °C (1st)/ 350 °C (solid line), Fe/ZSM5-He 350 °C (2nd)/350 °C (dotted line), Fe/ ZSM5-He 350 °C (3rd)/350 °C (dashed line), and Fe/ZSM5-He 350 °C/ LN (dashed-dotted line). Normalized XANES spectra of hematite (●, solid line) and Fe–titanate (○, solid line) are reported as internal Fe[III] and Fe[II] references. (b) Experimental $\chi(k)$ data of Fe/ZSM5-He 350 °C (1st)/350 °C (solid line), Fe/ZSM5-He 350 °C (2nd)/350 °C (dotted line), Fe/ZSM5-He 350 °C (3rd)/350 °C (dashed line). (c) Fourier transform (k^1, $\Delta k = 2.7$–13.2 Å^{-1}) of EXAFS data of Fe/ZSM5-He 350 °C (1st)/350 °C (solid line), Fe/ZSM5-He 350 °C (2nd)/350 °C (dotted line), Fe/ZSM5-He 350 °C (3rd)/350 °C (dashed line).

temperature. However, very important changes occurred during this stabilization period. The HR-XANES results (Fig. 1b) already showed that, after reaching 350 °C in He, the oxidation state of Fe is close to 2.4. The XANES spectra recorded in situ at 350 °C are depicted in Fig. 6a. The figure shows a clear shift to lower energy of the edge position of spectrum Fe/ZSM5-He 350 °C (1st)/350 °C, recorded after 30 min stabilization. This confirms that heating Fe/ZSM5 in He to 350 °C results in the reduction of a significant fraction of iron. However, the state of iron under He at 350 °C appeared to be unstable. This is visible by tracking the shift of the edge position with time on stream (measurements 1st, 2nd and 3rd). A significant shift ($+2$ eV) occurred, showing an average reoxidation of iron.

The effect of the reoxidation process on the local structure of iron can be tracked by the analysis of the EXAFS data collected in situ in He at 350 °C. The EXAFS spectra obtained respectively after 30, 60, and 90 min exposure to He are shown in Fig. 6b. It can be seen that both the amplitude and the nodes of the EXAFS oscillations are changing as a function of the stabilization period. The corresponding Fourier transforms are presented in Fig. 6c. The Fe–O contribution shows an increase with time on stream of its maximum intensity (at around 1.4 Å in the picture) accompanied by a contraction toward lower distance. No significant differences are visible, on the contrary, in the Fe–Fe contribution.

Table 5 shows the results of the EXAFS fit, performed on Fe/ZSM5 measured in situ at 350 °C during the stabilization in He. The most significant changes with time on stream occurred in the coordination number of the Fe–O_1 shell. The coordination number increased from 1.2 (1st scan) to 1.7 (3rd scan). As already deduced from the XANES spectra (Fig. 6a), this increase was accompanied by a corresponding partial oxidation of iron. The Fe–O_1 shell is therefore associated with the red–ox properties of the Fe-binuclear complexes. The decrease with time on stream of the coordination number of the Fe–O_3 shell, which was already shown not to be related to red–ox properties of iron (previous section), is most probably due to further desorption of water from the coordination sphere of iron. No differences were visible in the Fe–O_2 shell.

3.3.3. Heat treatment in O_2

The influence of the oxygen presence on the reducibility of iron during the heat treatment can be seen in Fig. 7a, by comparing the XANES spectra of Fe/ZSM5-He 350 °C (1st)/350 °C and Fe/ZSM5-O_2 350 °C/350 °C. As can be seen, the edge position of the sample heated in He (after 30 min stabilization) appears to be close to the edge of Fe–titanate (Fe[II]), while the edge position of Fe/ZSM5 heated in oxygen corresponds to that of the hematite reference (Fe[III]). Thus, oxygen prevented the auto-reduction of iron.

The XAFS spectra in the presence of oxygen were measured in situ (Fe/ZSM5-O_2 350 C/350°) and after cooling to 77 K (Fe/ZSM5-O_2 350 °C/LN). Differently from what

ARTICLE IN PRESS

S0021-9517(02)00188-4/FLA   AID:3950   Vol.●●●(●●●)
ELSGMLTM(JCAT):m5 2003/03/18 Prn:18/03/2003; 11:18

yjcat3950

P.10 (1-15)
by:Viktorija p. 10

10   A.A. Battiston et al. / Journal of Catalysis ●●● (●●●●) ●●●–●●●

Table 5
Coordination parameters (model 2:2:2) obtained by R-space analysis (k^1, $\Delta k = 2.7$–13.2 Å^{-1}; $\Delta R = 0.7$–4.2 Å) of EXAFS data of Fe/ZSM5-He 350 °C (1st)/350 °C, Fe/ZSM5-He 350 °C (2nd)/350 °C, Fe/ZSM5-He 350 °C (3rd)/350 °C, and Fe/ZSM5-He 350 °C/LN; $N_{indp} = 25.4$; $N_{free\,(fit)} = 22$

Shells	N	R (Å)	$\Delta\sigma^2$ (10^{-3} Å^2)	ΔE_0 (eV)	k^1-Variance (%)	
	($\pm10\%$)	($\pm1\%$)	($\pm5\%$)	($\pm10\%$)	Im. part	Abs. part
Fe/ZSM5-He 350 °C (1st)/350 °C					0.55	0.30
Fe–O$_1$	1.2	1.88	2.6	−5.5		
Fe–O$_2$	2.0	1.97	7.2	12.6		
Fe–O$_3$	1.2	2.08	8.8	−9.3		
Fe–Fe$_1$	1.1	2.99	13.0	0.4		
Fe–Fe$_2$	0.4	3.40	17.2	0.1		
Fe–O$_z$	1.6	4.09	15.0	−8.8		
Fe/ZSM5-He 350 °C (2nd)/350 °C					0.67	0.39
Fe–O$_1$	1.4	1.88	2.6	−5.5		
Fe–O$_2$	2.0	1.97	7.2	12.6		
Fe–O$_3$	1.1	2.08	8.8	−9.3		
Fe–Fe$_1$	1.1	2.99	13.0	0.4		
Fe–Fe$_2$	0.4	3.40	13.8	1.5		
Fe–O$_z$	2.2	4.00	15.0	−7.2		
Fe/ZSM5-He 350 °C (3rd)/350 °C					0.94	0.47
Fe–O$_1$	1.7	1.89	1.9	−6.5		
Fe–O$_2$	2.0	1.97	7.2	12.6		
Fe–O$_3$	0.7	2.06	2.0	−8.7		
Fe–Fe$_1$	1.2	2.97	12.5	−0.4		
Fe–Fe$_2$	0.4	3.40	14.8	3.1		
Fe–O$_z$	3.7	3.91	18.0	−2.2		
Fe/ZSM5-He 350 °C/LN					0.58	0.55
Fe–O$_1$	1.8	1.85	−3.5	−1.8		
Fe–O$_2$	2.0	1.97	−4.3	12.6		
Fe–O$_3$	0.9	2.08	2.2	−11.1		
Fe–Fe$_1$	1.2	2.97	1.3	1.8		
Fe–Fe$_2$	0.4	3.40	15.0	−5.5		
Fe–O$_z$	3.2	3.99	15.0	−4.9		

observed under helium, the three EXAFS spectra recorded in oxygen at high temperatures at increasing exposure time appeared to be identical and were therefore averaged. Significant differences are visible when comparing the EXAFS functions of Fe/ZSM5 measured in situ at 350 °C in oxygen, and in helium after 30 min stabilization (Fig. 7b). The corresponding Fourier transforms, collected in Fig. 7c, show that these differences concern mainly the Fe–O coordination. In the presence of oxygen, the Fe–O peak appears significantly enhanced in intensity and shifted towards lower R.

The structural parameters obtained by the analysis of the EXAFS spectra recorded in the presence of oxygen are collected in Table 6. Apart from differences in the Debye–Waller factors (temperature effects), the results of the fits (Fe/ZSM5-O$_2$ 350 °C/350 °C and Fe/ZSM5-O$_2$ 350 °C/LN) coincide. The total Fe–O coordination number (around 5.0) appears to be consistent with the results obtained by HR-XANES (see Fig. 2b (O$_2$, 350 °C)). When compared to the sample measured at 350° in He after 30 min stabilization (see Table 5), a sharp increase was detected in the coordination number of shell Fe–O$_1$ (1.9 vs
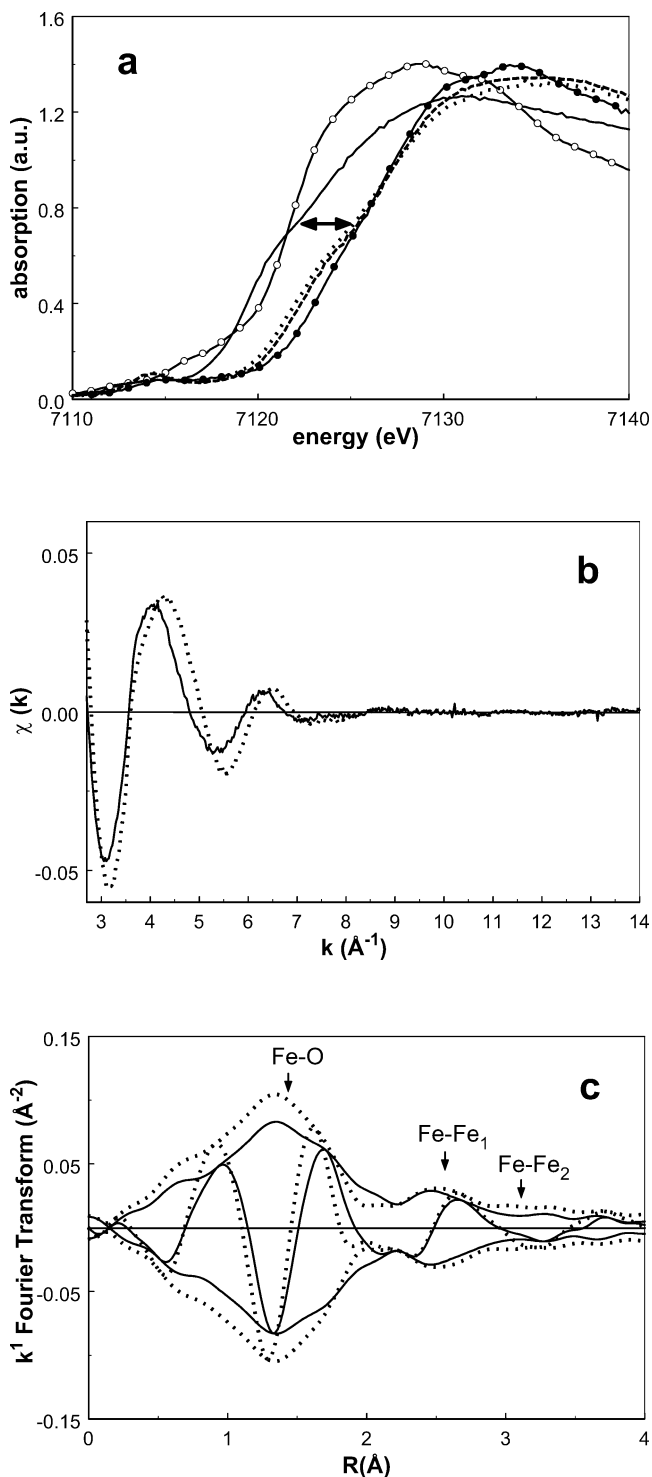

Fig. 7. (a) Normalized XANES spectra of Fe/ZSM5-He 350 °C (1st)/350 °C (solid line), Fe/ZSM5–O$_2$ 350 °C/350 °C (dotted line), and Fe/ZSM5–O$_2$ 350 °C/LN (dashed line). Normalized XANES spectra of hematite (●, solid line) and Fe–titanate (○, solid line) are reported as internal Fe^{III} and Fe^{II} references. (b) Experimental $\chi(k)$ data of Fe/ZSM5-He 350 °C (1st)/350 °C (solid line) and Fe/ZSM5–O$_2$ 350 °C/350 °C (dotted line). Note that the XAFS spectra of Fe/ZSM5 recorded at 350 °C in the presence of oxygen did not reveal any difference with time on stream. (c) Fourier transform (k^1, $\Delta k = 2.7$–13.2 Å^{-1}) of EXAFS data of Fe/ZSM5-He 350 °C (1st)/350 °C (solid line) and Fe/ZSM5–O$_2$ 350 °C/350 °C (dotted line).

ARTICLE IN PRESS

S0021-9517(02)00188-4/FLA   AID:3950   Vol.●●●(●●●)   P.11(1-15)
ELSGMLTM(JCAT):m5 2003/03/18 Prn:18/03/2003; 11:18   yjcat3950   by:Viktorija p. 11

A.A. Battiston et al. / Journal of Catalysis ●●● (●●●●) ●●●–●●●   11

Table 6
Coordination parameters (model 2:2:2) obtained by R-space analysis (k^1, $\Delta k = 2.7$–13.2 Å^{-1}; $\Delta R = 0.7$–4.2 Å) of EXAFS data of Fe/ZSM5-O$_2$ 350 °C/350 °C, and Fe/ZSM5-O$_2$ 350 °C/LN

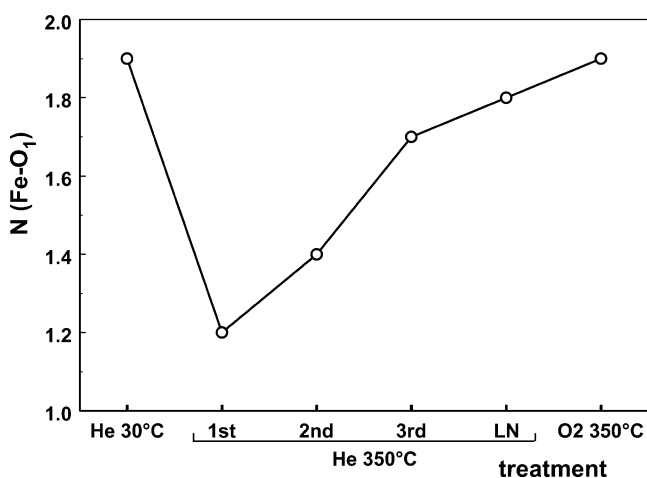| Shells	N	R (Å)	$\Delta\sigma^2$ (10^{-3} Å^2)	ΔE_0 (eV)	k^1-Variance (%)	
	($\pm10\%$)	($\pm1\%$)	($\pm5\%$)	($\pm10\%$)	Im. part	Abs. part
Fe/ZSM5-O$_2$ 350 °C/350 °C					1.26	0.50
Fe–O$_1$	1.9	1.86	2.0	−2.5		
Fe–O$_2$	2.0	1.99	5.0	13.0		
Fe–O$_3$	1.0	2.02	1.6	−13.3		
Fe–Fe$_1$	1.2	2.99	9.8	−1.6		
Fe–Fe$_2$	0.4	3.40	15.1	−3.7		
Fe–O$_z$	4.4	3.81	15.0	1.0		
Fe/ZSM5-O$_2$ 350 °C/LN					0.97	0.70
Fe–O$_1$	2.0	1.85	−3.8	−4.3		
Fe–O$_2$	2.0	1.97	−5.0	12.0		
Fe–O$_3$	1.0	2.02	4.5	−6.6		
Fe–Fe$_1$	1.2	2.96	2.4	2.0		
Fe–Fe$_2$	0.4	3.40	15.0	0.0		
Fe–Oz	3.8	3.91	15.0	−2.2		

$N_{\text{indp}} = 25.4$; $N_{\text{free (fit)}} = 22$.

Fig. 8. Number of oxygen atoms in the Fe–O$_1$ coordination shell (model 2:2:2) as a function of heat treatment in He, and in the presence of O$_2$.

1.2 for Fe/ZSM5-He 350 °C(1st)/350 °C). The coordination number of shell Fe–O$_3$, on the contrary, appears only slightly decreased, probably as a result of further water desorption with time on stream (1.0 vs 1.2, for Fe/ZSM5-He 350 °C(1st)/350 °C). The Fe–O$_3$ distance appears also to be slightly shortened. Also during the heating treatment in oxygen, the Fe–O$_2$ shell remained unaffected.

As shown by the results obtained during the heat treatments, changes in the oxidation state of iron are related to variations only in the Fe–O$_1$ coordination number. A coordination number of approximately 1 corresponds to an average Fe-oxidation state close to II. When the Fe–O$_1$ coordination number is increased to 2, Fe is completely oxidized (Fe^{III}). The changes in the Fe–O$_1$ coordination number, as a function of the different treatments, are visualized in Fig. 8.

As in the presence of helium, also the heat treatment in oxygen resulted in a shortening of the distance and a

decrease in the Debye–Waller factor of the Fe–Fe$_1$ shell (see for comparison Table 4, Fe/ZSM5-He 30 °C/LN). No differences were detected, on the other hand, in the coordination numbers of the Fe–Fe shells, excluding Fe–Fe agglomeration phenomena during the treatment.

4. Discussion

Several studies performed on Fe/ZSM5, obtained by CVD or solid-state ion exchange of FeCl$_3$, have elucidated the evolution of iron along the different steps of the synthesis [7,10,11,21,25,28,46], i.e., loading of iron, washing, and calcination. Upon sublimation of FeCl$_3$, iron is exchanged for the H$^+$ Brønsted protons of the zeolite in the form of isolated FeCl$_2{}^+$ species [25,28,46]. During the washing step, these species aggregate to form Fe-binuclear complexes, still bound to the framework aluminum [25,28]. The structure of the Fe-binuclear species in washed Fe/ZSM5, determined by EXAFS, resembles that of the closest Fe-binuclear building unit in α-goethite [30,31], consisting of octahedrally coordinated Fe^{III} oxo-hydroxo ions. A possible structure for the Fe-binuclear complexes, based on the similarity with the building blocks in α-goethite [30,31], was proposed in our previous study [25] and is depicted in Fig. 9a. In this model hydroxo-bridged Fe atoms are bound to the framework via two oxo-ions, and balance the lattice extra charge of two aluminum atoms. The Fe–O coordination, coherently with EXAFS and HR-XANES results, showing that iron possesses an octahedral coordination, is further completed by adsorbed water and by a terminal hydroxyl group. A similar model was presented by Marturano et al. [28], proposing a single oxo-bridge to the zeolite lattice.

The influence of calcination on the further evolution of the binuclear iron complexes was investigated in our previous work [25]. We have found that, if the calcination procedure is carefully controlled (mild calcination procedure), agglomeration of the binuclear Fe-complexes towards inactive oxidic clusters can be significantly suppressed, although not completely. This finding, based on HR-TEM, EELS, Mössbauer, FTIR, and EXAFS spectroscopy is confirmed by the results of the EXAFS analysis, presented in this work. Irrespective, to the different pretreatments applied (heating in He or O$_2$), two Fe–Fe shells could always be fitted, with a coordination number respectively of 1.2 and 0.4 (Tables 3–6). The closest Fe–Fe shell (Fe–Fe$_1$) is ascribed to the presence of binuclear Fe complexes [25,28]. The fact that the coordination number (N) of this shell is higher than 1.0, and that also a second Fe–Fe shell (Fe–Fe$_2$) could be fitted at a higher distance ($R = 3.40$ Å, $N = 0.4$), suggests that a fraction of iron possesses a higher degree of agglomeration than the binuclear complexes [25]. Nevertheless, from the EXAFS coordination numbers of the Fe–Fe shells, binuclear clusters in mildly calcined Fe/ZSM5 are estimated to account for at least 70% of the total iron. It should be noted that quantification by Mössbauer
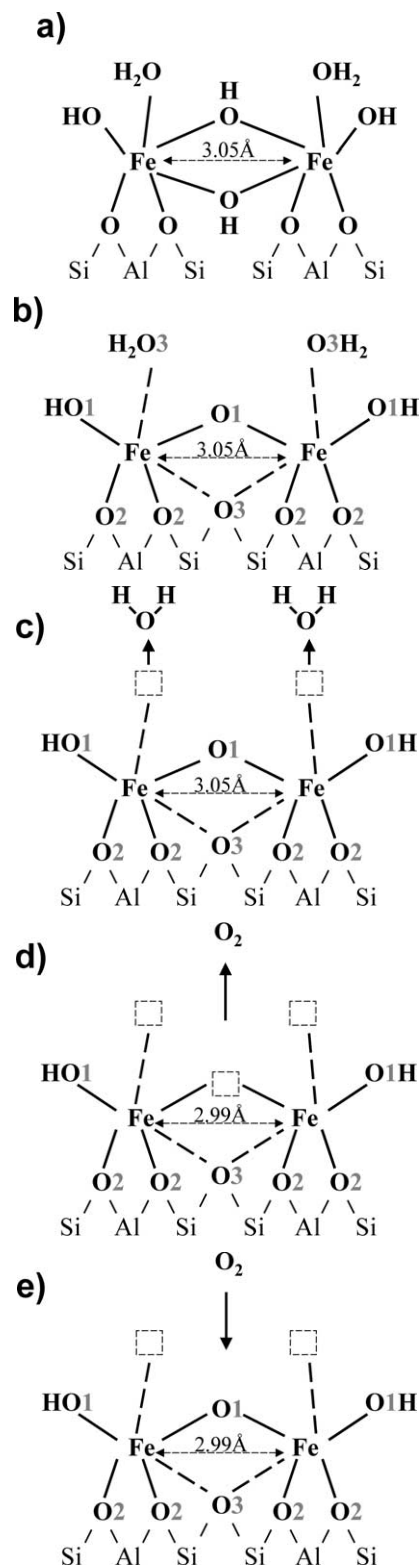
ARTICLE IN PRESS

S0021-9517(02)00188-4/FLA   AID:3950   Vol.●●●(●●●)
ELSGMLTM(JCAT):m5 2003/03/18 Prn:18/03/2003; 11:18

yjcat3950

P.12 (1-15)
by:Viktorija p. 12

12   *A.A. Battiston et al. / Journal of Catalysis ●●● (●●●●) ●●●–●●●*

Fig. 9. Proposed structure for the binuclear Fe complexes in Fe/ZSM5 obtained by CVD of FeCl₃ upon: (a) washing; (b) mild calcination and treatment in He at 30 °C; (c) mild calcination and moderate heating (up to ∼ 150 °C) in He or O₂/He (50:50): desorption of water; (d) mild calcination and heating in He to 350 °C: auto-reduction of iron, ascribed to the removal of the Fe–O–Fe bridging oxygen atom; (e) mild calcination and heating to 350 °C in a O₂/He (50:50) gas mixture: the presence of oxygen in the gas phase inhibits the removal of the Fe–O–Fe bridging oxygen atom.

spectroscopy has shown that this number could be over-estimated [25].

4.1. Binuclear iron complexes in mildly calcined Fe/ZSM5, pretreated in He at 30 °C

While calcination is generally applied as an activation procedure for Fe/ZSM5 obtained by CVD of FeCl₃ [10–12,25], its influence on the local Fe–O coordination of the Fe-binuclear complexes, formed upon washing, has not been unraveled, yet. The features of the Fe K pre-edge of (mildly calcined) Fe/ZSM5 measured in He at 30 °C (Fig. 1b) show that iron has a slightly distorted octahedral coordination and an oxidation state of III [35]. These results are confirmed by the position of the Fe K edge (Fig. 3a), which overlaps with that of the Fe^{III} hematite reference, and by the results of the EXAFS analysis (Table 3), showing the presence of six oxygen neighbors in the Fe-coordination sphere. The EXAFS data could be fitted with a symmetric oxygen distribution in two (model 3:3) or three (model 2:2:2) oxygen shells. A plausible structure for the binuclear Fe complexes in mildly calcined Fe/ZSM5 after pretreatment in He at 30 °C, arising from the EXAFS and the HR-XANES results, is depicted in Fig. 9b (oxygen atoms are labeled consistently with the 2:2:2 model in Table 3). This structure matches the model previously proposed in the literature [7,10,11,17] for the catalytically active phase in calcined Fe/ZSM5, i.e., a binuclear Fe complex with the core structure $[HO–Fe–O–Fe–OH]^{2+}$. This model is based on experimental evidence obtained by TPR, FTIR, and ESR studies [10–12,17] and appears as a plausible evolution of the binuclear complexes formed upon washing. The Fe–O–Fe bridging oxygen atom may result by the condensation at high temperature of two bridging hydroxyl groups with the desorption of a water molecule. A sufficient partial pressure of O₂ in the gas phase during calcination should prevent migration and desorption of the bridging oxygen.

In the model presented in Fig. 9b, the two oxygen atoms located by the EXAFS analysis in the closest oxygen shell (Fe–O₁) are assigned respectively to a bridging oxygen atom and a hydroxyl group. The Fe–O₁ distance (1.86 Å) appears to be consistent with the average distance of a terminal OH group and a Fe–O–Fe bridging oxygen. Molecular modeling calculations performed on a binuclear $[OH–Fe–O–Fe–OH]^{2+}$ model-complex, bound to the zeolite framework via two oxo-ions [47], have found for the terminal Fe–OH groups a distance of 1.88 Å and for the bridging Fe–O–Fe oxygen atom a Fe–O distance of 1.93 Å. Slightly shorter Fe–O distances are nevertheless reported in the literature for Fe–O–Fe oxo-bridges (around 1.85 Å) [48]. EXAFS is therefore not able to discriminate between these two types of oxygen. Oxygen located in shell Fe–O₂ is ascribed to two bridging (Fe–O–Al) O-atoms, by which the iron atoms are stabilized to the zeolite lattice. Indeed, the Fe–O₂ distance of 1.97 Å is consistent with the average distance found

for oxygen in the (Fe–O–Al) coordination of the mononuclear $FeCl_2^+$ complexes formed upon CVD of $FeCl_3$ [25,28]. In our previous work [25] we found a distance of 1.99 Å. Marturano et al. [28], though optimizing their EXAFS fit by introducing two separate Fe–O shells, found for the same Fe–O–Al coordination an average distance of 1.96 Å. Molecular modeling calculations, mentioned above, found for the Fe–O–Al bridges an average Fe–O distance of 1.95 Å, thus consistent with the $Fe–O_2$ shell assignment. The most distant oxygen, located in shell $Fe–O_3$, is assigned to weakly bound oxygen as in adsorbed water. As discussed further, since upon heating to 350 °C the C.N. of shell $Fe–O_3$ appeared to be reduced from 2 to only 1, oxygen atoms were not completely assigned to adsorbed water molecules. As depicted in Fig. 9b the second oxygen neighbor in $Fe–O_3$ was tentatively assigned to a Si–O–Si bridging oxygen of the zeolite framework.

4.2. Heat treatment in He (auto-reduction)

During heating in He different changes are revealed with increasing temperature in the Fe–O coordination of the Fe-binuclear complexes. Heating to 120 °C results in an increase of the integrated intensity of the Fe K pre-edge (Figs. 1a and b). This is the result of a decrease in the centrosymmetry of the coordination of the Fe atoms [35], caused by a lowering in the number of oxygen neighbors. The EXAFS fit reveals indeed a slight decrease, from 2.1 to 1.4, in the coordination number of the most distant Fe–O shell ($Fe–O_3$, Table 4). Shell $Fe–O_3$ therefore contains weakly bound oxygen, coherently with its elongated Fe–O bond. Since the decrease in the $Fe–O_3$ coordination number is not accompanied by a reduction in the oxidation state of iron, as revealed by the position of both the pre-edge centroid (Fig. 1b) and the Fe K edge (Fig. 3a), removal of oxygen up to 120 °C is ascribed exclusively to desorption of water, as depicted in Fig. 9c. No further changes are revealed in the results of the EXAFS fit. In particular, as already mentioned, no changes were visible in the fit of the Fe–Fe coordination, excluding further agglomeration of iron during heating.

An additional increase of the temperature under flowing helium caused clear changes in the features of the Fe K pre-edge (Figs. 1a and b), showing a clear reduction in the average oxidation state of iron. Indeed, the centroid position and the integrated intensity of Fe/ZSM5, already at 260 °C, correspond to those of a reference 50:50 $^{(6)}Fe^{III}/^{(4)}Fe^{II}$ physical mixture [35]. A slight additional reduction was revealed at 350 °C. The reduction is confirmed by the clear shift (∼ 4 eV) to lower energy of the Fe K edge (Fig. 6a).

These results show that, at high temperature in He, oxygen must be activated and removed from the Fe–O coordination of the binuclear complexes. Auto-reduction phenomena associated to desorption of oxygen at high temperature are known in the literature for Fe/ZSM5 prepared by CVD or solid-state ion exchange of $FeCl_3$. O_2-TPD experiments, performed by Voskoboinikov et al. [49] on

Fe/ZSM5 obtained by CVD on acidic supports with different Si/Al ratios, have shown that oxygen can be desorbed from Fe/ZSM5 by merely heating. Furthermore, the amount of oxygen released increases with decreasing Si/Al ratios. Lobree et al. [21] have come to similar conclusions studying the auto-reducibility of iron in Fe/ZSM5 obtained by solid-state ion exchange. They found that, at a fixed Si/Al ratio (S.A.R. was 25 in their experiments), the auto-reducibility of iron can be strongly enhanced by increasing the iron loading, i.e., by reducing the average distance of the iron atoms in the zeolite channels. Kucherov and Shelef [46] reached an identical conclusion using EPR spectroscopy. Activation of oxygen should therefore be facilitated by the close interaction of Fe atoms as in the case of Fe-binuclear clusters. The best suited candidate for the reactivity in He appears to be the bridging oxygen atom between the two Fe atoms. This hypothesis is supported by results obtained through $^{18}O_2$ isotopic exchange studies [26]. The experiments, performed on Fe/ZSM5 obtained by CVD, have shown a R1 isotopic exchange mechanism, prevailing at temperatures up to 450 °C, i.e., molecular oxygen from the gas phase exchanges only one ^{18}O atom against a ^{16}O atom from the solid. On Fe/ZSM5 obtained via impregnation, on the contrary, where the presence of binuclear complexes have been demonstrated to be negligible [26], a R2 mechanism prevails, in which $^{18}O_2$ is exchanged in one step against two ^{16}O atoms.

The analysis of the Fe/ZSM5 EXAFS data recorded in He at 350 °C (Fe/ZSM5-He 350 °C (1st)) shows that the reduction in the oxidation state of Fe is accompanied by a removal of oxygen from the closest Fe–O shell ($Fe–O_1$, Table 5). The coordination number of shell $Fe–O_1$ is reduced from 2.0 to 1.2, coherently with the removal of bridging Fe–O–Fe oxygen. Shell $Fe–O_2$ remains unmodified, confirming the correctness of its assignment to Fe–O–Al bridges, while only a slight further decrease is revealed in shell $Fe–O_3$. This is probably the result of further desorption of water with time on stream. A slight contraction is also visible in the Fe–Fe interatomic distance. By comparison with the Fe–Fe distance measured after cooling to 77 K (Fe/ZSM5-He 350 °C/LN, Table 4), the contraction cannot be ascribed to temperature effects and is probably the result of a rearrangement of the complexes upon heating. From the body of the HR-XANES and EXAFS results, the most plausible structure for the binuclear complexes in He at 350 °C is depicted in Fig. 9d. At this stage of the treatment two vacancies have been created in the coordination of iron by the desorption of respectively a weakly bound water molecule ($Fe–O_3$) and bridging oxygen ($Fe–O_1$). A discussion still open in the literature concerns the possibility of liberating gaseous O_2 by spatially separated oxo-complexes, such as $[HO–Fe–O–Fe–OH]^{2+}$, having only one bridging oxygen atom. Voskoboinikov et al. [26] have suggested that such complexes might communicate with each other via the O_2^- ions of the zeolite. Neighboring Fe–O–Fe complexes, separated by a limited number of O_2^-

ions of the support, could disproportionate into one Fe–O–O–Fe and one Fe–□–Fe complex, where □ stands for a vacancy. Oxygen could be subsequently easily desorbed by the (generated) highly unstable peroxo-complex. Such a mechanism would require the existence of Fe-binuclear complexes bound to pairs of Al-centered tetrahedra in close proximity with each other. This condition could indeed be fulfilled by a significant fraction of the iron complexes in over-exchanged Fe/ZSM5 (Fe/Al = 1) with a high Al/Si ratio.

Although a significant fraction of the Fe-binuclear complexes can undergo autoreduction in He at relatively low temperature ($\sim 250\,°C$), they appear to be highly unstable. This was revealed by the differences in the XAFS spectra recorded with time on stream at $350\,°C$ and at 77 K after 120 min stabilization in He at $350\,°C$. As seen in Fig. 6a, the Fe K edge appeared to be shifted stepwise to higher energy with exposure time, thus reoxidation of iron took place during the measurements. The reoxidation was accompanied by a reincrease in the coordination number of shell Fe–O_1 (Table 5). The remaining shells, on the contrary, remained virtually unchanged. This result confirms the previous observation that changes in the oxidation state of iron are related to only one oxygen atom in the closest Fe–O shell (Fe–O_1), most probably the Fe–O–Fe bridging atom. The reason for the reoxidation with time on stream is still unclear. While He with a very high purity was used (certified purity 5.0), additional oxygen traps were not added to the He line. It can therefore not be excluded that traces of oxygen from the gas phase might have partially reoxidized the Fe complexes. Nevertheless, reoxidation could also have been caused by oxygen released at high temperatures from the zeolite, supporting the idea of Voskoboinikov et al. [26] of an easy oxygen exchangeability between the zeolite and the Fe-binuclear complexes.

4.3. Heat treatment in the presence of O_2

Up to a moderate temperature, the addition of oxygen to the helium flow does not cause significant changes to the coordination of iron. Heating Fe/ZSM5 to $160\,°C$ in oxygen results in an increase of the Fe K pre-edge intensity (Figs. 2a and b) similar to that measured in He at $130\,°C$ (Fig. 1a and b). As in the case of He, this is ascribed to desorption of water, coordinated to the binuclear complexes upon exposure of the Fe/ZSM5 sample to air. As expected, desorption of water is not influenced by the presence of oxygen (Fig. 9c).

On the contrary, changes occurring to the binuclear complexes at higher temperatures (from 130 to $350\,°C$) appeared to be strongly influenced by the presence of oxygen in the gas phase. As seen from Fig. 2b, which collects the pre-edge features of Fe/ZSM5 heated in oxygen, the oxidation state of iron remained unchanged (Fe[III]) up to $350\,°C$. This result is confirmed by the position of the Fe K edge, which overlaps with that of the hematite reference and of Fe/ZSM5 measured at $30\,°C$ (Fig. 7a). These results

show that the presence of oxygen in the gas phase ($P_{O_2} = 0.5$ bar) suppresses the autoreduction capability revealed by the binuclear complexes at the same temperature in He. The intensity of the Fe K pre-edge in oxygen at $350\,°C$ is similar to that of the five-fold coordinated Fe[III] reference (Fig. 2b) [35]. Consistently, five oxygen neighbors have been identified by the EXAFS analysis (Table 6). As at $350\,°C$ in helium, only one oxygen is located in the Fe–O_3 shell, in agreement with the removal of one water molecule during heating. The distance of the remaining oxygen in the Fe–O_3 shell appears to be slightly shortened, pointing to a stronger bond of the Fe to the zeolite Si–O–Si oxygen. Shell Fe–O_2, assigned to two oxygen atoms of Fe–O–Al bridges, remained unchanged, consistently with the assignment. As can be seen also qualitatively, by comparing the k^1 Fourier transforms depicted in Fig. 7c, the difference in the Fe–O coordination of the binuclear complexes at $350\,°C$ in the presence or absence of oxygen are localized at low R. The EXAFS analysis revealed, indeed, that different from the measurement in He at $350\,°C$, in the presence of oxygen the coordination number of the Fe–O_1 shell remains 2, as it was in Fe/ZSM5 measured in He at $30\,°C$. This result confirms that the Fe[II] $\leftrightarrow$ Fe[III] red–ox reversibility in the binuclear complexes is related to one oxygen atom located in shell Fe–O_1 ($R = 1.86\,Å$). According to the model proposed by Chen et al. [10–12] this atom is assigned to a Fe–O–Fe bridging oxygen (Fig. 9e). In the presence of a significant partial pressure of oxygen in the gas phase its removal (desorption) from the Fe complexes appears to be inhibited.

5. Conclusions

The analysis of the EXAFS and HR-XANES data obtained from mildly calcined Fe/ZSM5 shows that the majority of iron is present as Fe oxo-hydroxo binuclear complexes. The closest Fe–O coordination of the Fe-binuclear complexes can be described with a $[HO–Fe–O–Fe–OH]^{2+}$ core.

Heat treatments to $350\,°C$ in He and in a 50:50 O_2/He mixture do not cause further agglomeration of iron. Heating to a moderate temperature (up to $\sim 150\,°C$) results in the desorption of water from the Fe coordination sphere. As expected, desorption of water is unaffected by the composition of the gas phase (He or a 50:50 O_2/He mixture).

On the contrary, the composition of the gas phase strongly influences the changes occurring to the binuclear complexes in the $150–350\,°C$ temperature range. By heating in He a significant fraction of iron is reduced (auto-reduction). This is accompanied by the removal of approximately one oxygen atom from the closest Fe–O shell, attributed to the Fe–O–Fe bridging oxygen atom. The reduced binuclear complexes appear to be highly unstable and undergo reoxidation with time on stream.

ARTICLE IN PRESS

S0021-9517(02)00188-4/FLA   AID:3950   Vol.●●●(●●●)
ELSGMLTM(JCAT):m5 2003/03/18 Prn:18/03/2003; 11:18

yjcat3950

P.15 (1-15)
by:Viktorija p. 15

A.A. Battiston et al. / Journal of Catalysis ●●● (●●●●) ●●●–●●●

15

The presence of oxygen in the gas phase ($P_{O_2} = 0.5$ bar) suppresses the auto-reduction capability of the binuclear complexes by inhibiting the removal of the Fe–O–Fe bridging oxygen.

References

[1] G.I. Panov, A. Kharitonov, V. Sobolev, Appl. Catal. 98 (1993) 1.

[2] G.I. Panov, V. Sobolev, K.A. Dubkov, V.N. Parmon, N.S. Ovanesyan, A.E. Shilov, A.A. Shteinmann, React. Kinet. Catal. Lett. 61 (1997) 251.

[3] G.I. Panov, A.K. Uriarte, M.A. Rodkin, V.I. Sobolev, Catal. Today 41 (1998) 365.

[4] G.I. Panov, Cattech. 4 (2000) 18.

[5] A. Ribera, I.W.C.E. Arends, S. de Vries, J. Pérez-Ramírez, R.A. Sheldon, J. Catal. 195 (2000) 287.

[6] F. Kapteijn, G. Marbán, J. Rodríguez-Mirasol, J.A. Moulijn, J. Catal. 167 (1997) 256.

[7] E.M. El-Malki, R.A. van Santen, W.M.H. Sachtler, J. Catal. 196 (2000) 212.

[8] J. Pérez-Ramírez, F. Kapteijn, G. Mul, J.A. Moulijn, Chem. Commun. 693 (2001).

[9] J. Pérez-Ramírez, F. Kapteijn, G. Mul, J.A. Moulijn, Appl. Catal. B 35 (2001) 227.

[10] H.Y. Chen, W.M.H. Sachtler, Catal. Today 42 (1998) 73.

[11] H.-Y. Chen, T. Voskoboinikov, W.M.H. Sachtler, J. Catal. 180 (1998) 171.

[12] H.-Y. Chen, T. Voskoboinikov, W.M.H. Sachtler, Catal. Today 54 (1999) 483.

[13] J. Pérez-Ramírez, G. Mul, F. Kapteijn, J.A. Moulijn, A.R. Overweg, A. Doménech, A. Ribera, I.W.C.E. Arends, J. Catal. 207 (2002) 113.

[14] N.S. Ovanesyan, A.A. Shteinman, V.I. Sobolev, K.A. Dubkov, G.I. Panov, Kinet. Katal. 39 (1998) 863.

[15] M.A. Rodkin, V.I. Sobolev, K.A. Dubkov, N.H. Watkins, G.I. Panov, Stud. Surf. Sci. Catal. 130 (2000) 875.

[16] K.A. Dubkov, N.S. Ovanesyan, A.A. Shteinman, E.V. Starokon, G.I. Panov, J. Catal. 207 (2002) 341.

[17] H.-Y. Chen, E.M. El-Malki, X. Wang, R.A. van Santen, W.M.H. Sachtler, J. Mol. Catal. A 162 (2000) 159.

[18] X. Feng, W.K. Hall, J. Catal. 166 (1997) 368.

[19] M. Kögel, V.H. Sandoval, W. Schwieger, A. Tissler, T. Turek, Catal. Lett. 51 (1998) 23.

[20] R. Joyner, M. Stockenhuber, J. Phys. Chem. B 103 (1999) 5963.

[21] L.J. Lobree, I.-C. Hwang, J.A. Reimer, A.T. Bell, J. Catal. 186 (1999) 242.

[22] B.R. Wood, J.A. Reimer, A.T. Bell, J. Catal. 209 (2002) 151.

[23] F. Heinrich, C. Schmidt, E. Löffler, W. Grünert, Catal. Commun. 2 (2001) 317.

[24] M. Kögel, R. Mönnig, W. Schwieger, A. Tissler, T. Turek, J. Catal. 182 (1999) 470.

[25] A.A. Battiston, J.H. Bitter, F.M.F. de Groot, A.R. Overweg, O. Stephan, J.A. van Bokhoven, P.J. Kooyman, C. van der Spek, G. Vankó, D.C. Koningsberger, J. Catal. 213 (2003) 251.

[26] T.V. Voskoboinikov, H.-Y. Chen, W.M.H. Sachtler, J. Mol. Catal. A 155 (2000) 155.

[27] P. Marturano, L. Drozdová, A. Kogelbauer, R. Prins, J. Catal. 192 (2000) 236.

[28] P. Marturano, L. Drozdová, G.D. Pirngruber, A. Kogelbauer, R. Prins, Phys. Chem. Chem. Phys. 3 (2001) 5585.

[29] A.A. Battiston, J.H. Bitter, D.C. Koningsberger, Catal. Lett. 66 (2000) 75.

[30] J.R. Rustad, A.R. Felmy, B.P. Hay, Geochim. Cosmochim. Acta 90 (1996) 1553.

[31] S. Suzuki, T. Suzuki, M. Kimura, Y. Takagi, K. Shinoda, K. Tohji, Y. Waseda, App. Surf. Science 109 (2001) 169–170.

[32] G. Dräger, R. Frahm, G. Materlik, O. Brummer, Phys. Stat. Sol. B 146 (1988) 287.

[33] D. Heumann, G. Dräger, S. Bocharov, J. Physique IV 7C2 (1997) 481.

[34] T.E. Westre, P. Kennepohl, J. de Witt, B. Hedman, K.O. Hogson, E.I. Solomon, J. Am. Chem. Soc. 119 (1997) 6297.

[35] M. Wilke, F. Farges, P.-E. Petit, G.E. Brown Jr., F. Martin, Am. Miner. 86 (2001) 714.

[36] F. Sette, G. Ruocco, M. Krisch, U. Bergmann, C. Masciovecchio, V. Mazzacurati, G. Signorelli, R. Verbeni, Phys. Rev. Lett. 75 (1995) 850.

[37] M. Vaarkamp, B.L. Mojet, F.S. Modica, J.T. Miller, D.C. Koningsberger, J. Phys. Chem. 99 (1995) 16067.

[38] S.L.M. Schroeder, Adv. Spectrosc. 26 (1998) 1.

[39] M. Vaarkamp, J.C. Linders, D.C. Koningsberger, Physica B 209 (1995).

[40] M. Vaarkamp, I. Dring, R.J. Oldman, E.A. Stern, D.C. Koningsberger, Phys. Rev. B 50 (1994) 7872.

[41] D.C. Koningsberger, B.L. Mojet, G.E. van Dorssen, D.E. Ramaker, Top. Catal. 10 (2000) 143.

[42] J.W. Cook, D.E. Sayers, J. Appl. Phys. 52 (1981) 5024.

[43] A.L. Ankudinov, J.J. Rehr, Phys. Rev. B 56 (1997) R1712.

[44] D.C. Koningsberger, Jpn. J. Appl. Phys. 32 (1993) 877.

[45] G.G. Li, F. Bridges, C.H. Booth, Phys. Rev. B 52 (1995) 6332.

[46] A.V. Kucherov, M. Shelef, J. Catal. 195 (2000) 112.

[47] A.A. Battiston, D. de Romph, F.M.F. de Groot, J.H. Bitter, D.C. Koningsberger, manuscript in preparation.

[48] H.F. Hsu, Y. Dong, L. Shu, V.G.J. Young, L.J. Que, J. Am. Chem. Soc. 121 (1999) 5230.

[49] T.V. Voskoboinikov, H.-Y. Chen, W.M.H. Sachtler, Appl. Catal., B 19 (1998) 279.